

CrystEngComm

Accepted Manuscript



This is an *Accepted Manuscript*, which has been through the Royal Society of Chemistry peer review process and has been accepted for publication.

Accepted Manuscripts are published online shortly after acceptance, before technical editing, formatting and proof reading. Using this free service, authors can make their results available to the community, in citable form, before we publish the edited article. We will replace this *Accepted Manuscript* with the edited and formatted *Advance Article* as soon as it is available.

You can find more information about *Accepted Manuscripts* in the [Information for Authors](#).

Please note that technical editing may introduce minor changes to the text and/or graphics, which may alter content. The journal's standard [Terms & Conditions](#) and the [Ethical guidelines](#) still apply. In no event shall the Royal Society of Chemistry be held responsible for any errors or omissions in this *Accepted Manuscript* or any consequences arising from the use of any information it contains.

In Situ Generation of Functionality in a Reactive Binicotinic-Acid-Based Ligand for the Design of Multi-Functional Copper(II) Complexes: Syntheses, Structures and Properties

Dongsheng Deng,^a Hui Guo,^a Guohui Kang,^{a,b} Lufang Ma,^a Xu He,^a Baoming Ji^{a*}

^a College of Chemistry and Chemical Engineering, Luoyang Normal University,
Luoyang 471022, P. R. China

^b College of Chemistry and Chemical Engineering, Zhengzhou University, Zhengzhou
450052, P. R. China.

ABSTRACT: Under hydrothermal conditions, including tuning the reaction ratio and reaction temperature, three-dimensional (3D) porous $\{[\text{Cu}_3(\text{hbpdc})(\text{OH})_2(\text{H}_2\text{O})]\cdot 2\text{H}_2\text{O}\}$ (**1**), two-dimensional (2D) sheet $\{\text{Cu}_2(\text{hbpdc})(\text{H}_2\text{O})_2\}_n$ (**2**), dinuclear $[\text{Cu}(\text{hbpdc})_{0.5}(\text{H}_2\text{O})_2]$ (**3**), dimer $[\text{Cu}_2(\text{mbpdc})_2(\text{py})_2]\cdot 9\text{H}_2\text{O}$ (**4**), and mononuclear $[\text{Cu}(\text{hbpdcH}_2)(\text{H}_2\text{O})_2]$ (**5**) have been synthesized via in situ ligand transformation reaction, in which 3,3'-dimethoxy-2,2'-bipyridine-6,6'-dicarboxylic acid (mbpdcH₂) undergoes demethylation to 3,3'-dihydroxy-2,2'-bipyridine-6,6'-dicarboxylic acid (hbpdcH₄). The detailed coordination patterns of hbpdcH₄ ligand have been revealed by single-crystal X-ray diffraction. The catalytic results demonstrate that polymers **1** and **2** can function as heterogeneous and reusable catalysts for the Strecker reaction of various imines. In addition, magnetic susceptibility measurements of complexes **1**, **2** and **4** reveal antiferromagnetic coupling between the copper(II) ions. Complex **1** follows the Curie-Weiss law, while **2** and **4** obey the Bleaney-Bowers dinuclear model.

INTRODUCTION

As a flourishing research field, metal-organic hybrid materials (MOHM), containing paramagnetic metal ions incorporated into coordination polymers to fabricate extended structures, are currently of significant interest in materials chemistry, not only because of their fascinating structural diversities, but also for their useful properties and promising application in the field of gas storage, separation, magnetism, and catalysis.¹ In general, such MOHM are typically composed of organic ligands as linkers and metal ions or metal ion clusters as nodes.² The

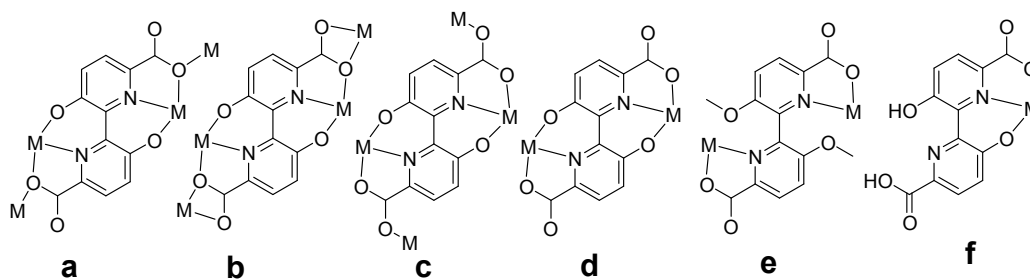
assembly of reaction components from solution to the solid state can be achieved through various means, and each of these pathways can afford unique materials. In this respect, much effort has been directed toward developing the ability to control the reactions so that the products can be engineered to have desired properties.³ Although remarkable progress in this area has been achieved, the rational design and synthesis of MOHMs with unique structure and function still remain a significant challenge. Many factors such as nature of the metal ion,⁴ structural features of the organic ligand,⁵ counterions,⁶ temperature,⁷ reagent ratio,⁸ pH value,⁹ *etc.*, can exert great impacts on the final architectures. With respect to temperature, its effect on forming the coordination polymers has not been intensively explored, though some reports described how the reaction temperature affects the generation of different coordination polymers.^{7,10}

Currently, multidentate N- and O-donor bridging ligands have been widely used to construct MOHMs, due to their wide range of binding, modes that provide supper exchange pathways for magnetic coupling among paramagnetic metal centers.^{11,12} Thus, inorganic-organic hybrid materials formed with pyridine-, pyrazine-, pyrimidine-, and imidazole-carboxylic acid, *etc.*, as linkers are known in the literature.¹³ In this regard, binicotinic acids and its derivatives are excellent candidates for the construction of novel intriguing structures and topologies, because they have multiple coordination sites and can adopt more versatile conformations.^{14,15}

In addition to magnetic properties, inorganic-organic hybrid materials have provided a tunable platform for the design of heterogeneous catalysts due to their high surface areas inside the pores and uniform catalytic sites (both metal ions and linkers can act as catalytic sites).^{16,16} Some MOHMs have open metal sites which exhibit Lewis acidity and could catalyze organic reactions such as cyanosilylation of aldehyde or ketone, Mukayama aldol reaction, ring-opening of epoxides and Friedel-Crafts alkylation reaction, *etc.*¹⁷

In the light of above-mentioned facts, we are here to focus our attention on using a 3,3'-dimethoxy-2,2'-bipyridine-6,6'-dicarboxylic acid, as multidentate ligand to construct functional materials, which is based on the following considerations: 1) the two carboxylic hydrogen atoms can be easily deprotonated, allowing the four carboxylate oxygen atoms to bind to two or three or four metal centers, as observed in other binicotinic acid ligands;^{14,15} 2) when two methoxy groups hydrolyzed to hydroxyl groups through an in situ ligand transformation reaction under hydrothermal conditions, the resulting 3,3'-dihydroxy-2,2'-bipyridine-6,6'-dicarboxylic acid

ligand displays multidentate coordination modes, as depicted in Scheme 1a-1f. The carboxylate oxygen can form a chelating bond to a metal center with the adjacent hydroxyl oxygen and pyridyl nitrogen. Consequently, the hbpdc⁴⁻ ligand, with multifunctional coordination sites, is an effective component in the design of a diverse range of functional coordination complexes. On the basis of the above analysis, we first synthesized a 3D porous MOFs, {[Cu₃(hbpdc)(OH)₂(H₂O)]·2H₂O} (**1**).^{14d} Next, we synthesized another four complexes: {Cu₂(hbpdc)(H₂O)₂}_n (**2**), [Cu(hbpdc)_{0.5}(H₂O)₂] (**3**), [Cu₂(mbpdc)₂(py)₂]·9H₂O (**4**), and [Cu(hbpdcH₂)(H₂O)₂] (**5**) by using mbpdcH₂ ligand with the help of different reaction conditions including reaction temperature and reactant ratio. The crystal structures and coordination modes of hbpdcH₄, along with the regulatory effect of reaction conditions for these complexes, have been analyzed. The magnetic properties of complexes **1**, **2** and **4** have been investigated. In addition, the heterogeneous catalytic activities of complexes **1** and **2** for the Strecker reactions of various imines in aqueous media have also been investigated.



Scheme 1. The coordination modes of the hbpdcH₄ ligand in complexes **1–5**.

EXPERIMENTAL SECTION

Material and General Methods. The reagents need for synthesis were used as received. 3,3'-dimethoxy-2,2'-bipyridine-6,6'-dicarboxylic acid was prepared according to the literature method.^{14d} The C, H, and N microanalyses were carried out on a Flash 2000 elemental analyzer. IR Spectra were recorded as KBr pellets on a Nicolet Avatar-360 spectrometer in the 4000-400. TG-DSC measurements were performed by heating the crystalline sample from 25 to 900 °C at a rate of 2 °C/min in a N₂ atmosphere on a SDTQ600 differential thermal analyzer. Powder X-ray diffractometer were performed on a Bruker D8-ADVANCE X-ray diffractometer operated using a 0.02° step scan from 5 to 50°C in 2θ and 0.2 s preset time. ¹H NMR spectra were recorded on a

Bruker DPX-400 spectrometer in CDCl₃ with TMS as an internal standard. Variable-temperature magnetic susceptibilities were measured with an MPMS-7 SQUID magnetometer. Diamagnetic corrections were made with Pascal's constants for all constituent atoms.

Synthesis of polymer 1 ($\{[\text{Cu}_3(\text{hbpdc})(\text{OH})_2(\text{H}_2\text{O})]\cdot 2\text{H}_2\text{O}\}_n$)

Polymer **1** was prepared according to the literature method.^{14d} A total of 0.2 mmol (63.5 mg) of mbpdcH₂ and 0.4 mmol (79.9 mg) of Cu(CH₃COO)₂·4H₂O in a molar ratio of 1:2 were combined with 13 mL of deionized water in a 15 mL stainless steel bomb. This was sealed and heated at 160 °C for 4 days, then cooled to room temperature at a rate of 5 °C h⁻¹. Blue block crystals suitable for X-ray single crystal analysis were obtained in 81% yield (base on Cu). These crystals were separated, washed with water, and dried under ambient conditions.

Synthesis of polymer 2 $\{\text{Cu}_2(\text{hbpdc})(\text{H}_2\text{O})_2\}_n$

Polymer **2** was obtained by the same method as that of **1** except that reaction temperature was changed from 160 to 140 °C. After being cooled to room temperature, blue crystals were obtained in 85%. Anal. Calcd. For C₁₂H₈Cu₂N₂O₈: C, 33.11; H, 1.85; N, 6.44%. Found: C, 33.18; H, 1.96; N, 6.49%. IR (KBr, cm⁻¹): 3416(s), 3138(m), 1651(m), 1576(s), 1424(m), 1362(s), 1318(m), 1120(m), 877(m), 863(m), 797(s), 699(s).

Synthesis of complex 3 $[\text{Cu}(\text{hbpdc})_{0.5}(\text{H}_2\text{O})_2]$

Complex **2** was synthesized by the same procedure used for preparing **1** except that metal-to-ligand ratio was altered from 1:2 to 2:1. After being cooled to room temperature, blue crystals were obtained in 20% yield. Anal. Calcd. For C₆H₆CuNO₅: C, 30.58; H, 2.57; N, 5.94%. Found: C, 30.66; H, 2.69; N, 5.99%. IR (KBr, cm⁻¹): 3418(m), 3041(s), 2950(m), 1697(s), 1634(s), 1567(m), 1492(m), 1422(s), 1359(s), 1289(s), 1242(m), 1172(m), 912(s), 863(s), 851(m), 790(s), 715(m).

Synthesis of complex (4) $[\text{Cu}_2(\text{mbpdc})_2(\text{py})_2]\cdot 9\text{H}_2\text{O}$

Complex **4** was prepared by a similar procedure as that for **1** except that metal-to-ligand ratio was altered from 1:2 to 1:1, and the use pyridine as the additives. After being cooled to room temperature, blue crystals were obtained in 70% yield. Anal. Calcd. For C₃₈H₄₈Cu₂N₆O₂₁: C, 43.39; H, 4.60; N, 7.99%. Found: C, 43.52; H, 4.72; N, 8.15%. IR (KBr, cm⁻¹): 3453(m), 2965(w), 2933(w), 2863(w), 1639(s), 1568(m), 1429(s), 1389(s), 1337(m), 1225(m), 1124(m), 893(m), 854(m), 788(m), 709(m).

Synthesis of complex (5) [Cu(hbpdCH₂)(H₂O)₂]

The preparation of **5** was similar to that of **1** except that metal-to-ligand ratio was altered from 1:2 to 1:1. After being cooled to room temperature, blue crystals were obtained in 70% yield. Anal. Calcd. For C₁₂H₁₀CuN₂O₈: C, 38.56; H, 2.70; N, 7.49%. Found: C, 38.69; H, 2.86; N, 7.62%. IR (KBr, cm⁻¹): 3418(w), 3041(s), 2950(m), 1697(s), 1634(s), 1567(m), 1492(m), 1422(s), 1359(s), 1289(s), 1242(m), 1172(m), 912(s), 863(s), 851(m), 790(s), 715(m).

Single-Crystal Structure Determination. A suitable single crystal was carefully selected under a polarizing microscope and glued carefully to a thin glass fiber. Crystallographic data of **1–5** were collected on a Bruker Smart Apex-II CCD area detector equipped with a graphite-monochromatic Mo K α radiation ($\lambda = 0.71073 \text{ \AA}$) at room temperature. Data were reduced using SAINTPLUS, and an empirical absorption correction was applied using the SADABS program. The structure were solved with direct methods and refined with full-matrix least-squares techniques on F^2 using the SHELXTL program package.^{18,19} The non-hydrogen atoms were placed in geometrically ideal positions and refined as riding atoms with a common isotropic thermal parameter. Detail of the structure solution and final refinements are given in Table 1. CCDC 96844 (1), 968446 (2), 968447 (3), 968448 (4) and 968449 (5) contain the supplementary crystallographic data. These data can be obtained free of charge via www.ccdc.cam.ac.uk/conts/retrieving.html (or from the Cambridge Crystallographic Data Center, 12 Union Road, Cambridge CB2 1EZ, UK; fax: (44) 1223 336-033. Email: deposit@ccdc.cam.ac.uk

Catalysis Experiments. Polymers **1** and **2** were activated at 120 °C for 8 h under vacuum before the reaction was carried out. A typical Strecker reaction procedure was performed as follows: A quantity of 24 mg (0.005 mmol of **1**) of catalyst was suspended in dry CH₂Cl₂ (2 mL) followed by the addition of imines (0.1 mmol) and trimethylsilyl cyanide (0.15 mmol). The reaction mixtures were stirred for 4 h at 298 K under N₂. Catalytic recyclability was checked for four times with the same batch of catalyst. The recovered catalysts were characterized by the X-ray powder diffraction and showed identical results to those of the fresh samples.

Table 1. Crystallographic data and structure refinement summary for complexes 1–5

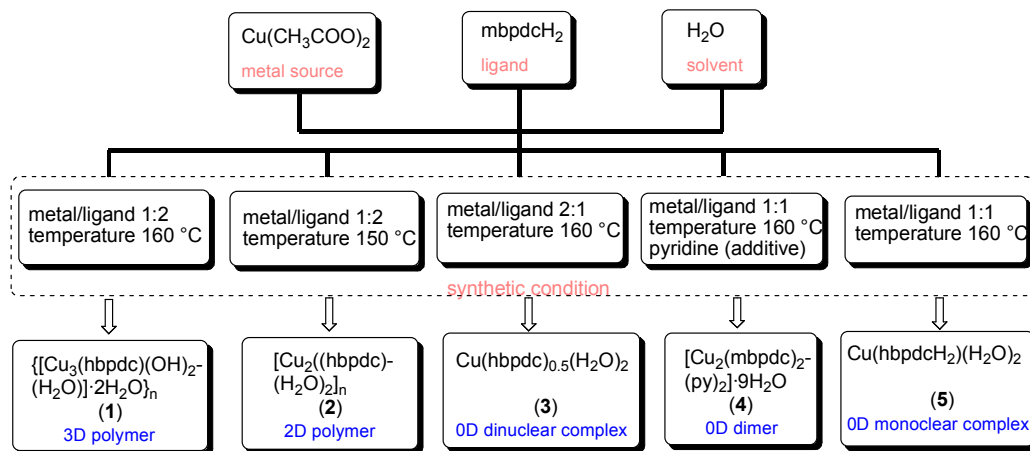
Complexes	1	2	3	4	5
Chemical formula	C ₁₂ H ₁₀ Cu ₃ N ₂ O ₁₀	C ₁₂ H ₈ Cu ₂ N ₂ O ₈	C ₆ H ₆ CuNO ₅	C ₃₈ H ₄₈ Cu ₂ N ₆ O ₂₁	C ₁₂ H ₁₀ CuN ₂ O ₈
Formula weight	532.84	435.28	235.66	1051.90	373.76
Crystal system	Monoclinic	Monoclinic	Triclinic	Triclinic	Triclinic
Space group	<i>C2/c</i>	<i>P2₁/c</i>	<i>P</i> $\bar{1}$	<i>P</i> $\bar{1}$	<i>P</i> $\bar{1}$
<i>a</i> /Å	16.892(3)	18.211(3)	6.2937(16)	12.1868(13)	4.785(7)
<i>b</i> /Å	15.722(2)	5.1283(10)	6.8393(17)	12.4222(13)	9.330(14)
<i>c</i> /Å	5.8595(9)	13.915(3)	9.545(4)	15.4307(16)	14.53(2)
α /°	90	90	99.689(4)	77.399(10)	89.807(16)
β /°	106.112(2)	96.803(2)	90.764(4)	88.583(10)	81.067(16)
γ /°	90	90	116.946(3)	85.884(10)	77.496(16)
Volume/Å ³	1495.0(4)	1290.4(4)	359.14(19)	2273.8(4)	625.4(16)
<i>Z</i>	4	4	1	2	2
<i>D</i> _{calc} /g cm ⁻³	2.367	2.241	2.179	1.536	1.985
μ /mm ⁻¹	4.294	3.348	3.027	2.274	1.798
<i>T</i> /K	293(2)	294(2)	293(2)	291(2)	296(2)
Reflns. Collected	5230	8900	2762	17105	4758
Unique reflns	1388	2395	1333	8423	2309
<i>R</i> _{int}	0.0272	0.0295	0.0215	0.0265	0.0203
Goodness-of-fit	1.029	1.022	1.073	1.030	1.058
<i>R</i> ₁ (<i>I</i> > 2 σ)	0.0244	0.0296	0.0338	0.0395	0.0282
<i>wR</i> ₂ (<i>I</i> > 2 σ)	0.0611	0.0724	0.0813	0.0981	0.0750

RESULTS AND DISCUSSION

Synthesis and Spectroscopic Characterization

As is well known, in situ ligand transformation reaction may occur during hydrothermal reaction, which is currently regarded as an effective strategy to obtain novel MOHMs that are inaccessible or not easily achieved by the conventional methods.²⁰ However, the controlled synthesis of MOHMs is still a major challenge.²¹ Small changes in one or more of the variables of hydrothermal reaction such as temperature, metal-to-ligand ratio, and pH value, have a profound influence on the final crystallization outcome.²² As far as these factors are concerned, complexes **1–5** were successfully obtained by the in situ reaction of mbpdcH₂ with Cu(II) acetate through tuning hydrothermal temperature, metal-to-ligand ratio and additive. The self-assembly strategies

are given in Scheme 2. On the basis of identical reactants, the structures of **1** and **2** differed in the case of altered reaction temperature. Complexes **3** and **5** were obtained by changing metal-to-ligand ratio. Finally, complex **4** can be obtained by altering metal-to-ligand ratio in the addition of pyridine.



Scheme 2. Self-Assembly Syntheses of **1–5**

Description of crystal structures.

Crystal structure of 1.

Under 160 °C hydrothermal conditions, the reaction of Cu(II) acetate with mbpdcH₂ ligand can afford polymer **1** with metal-to-ligand ratio of 2:1. The polymer **1** features a highly ordered 3D nanoporous structure encapsulating a ZigZag water chain. The detail structural discussion of **1** has been reported in our previous paper.^{14d}

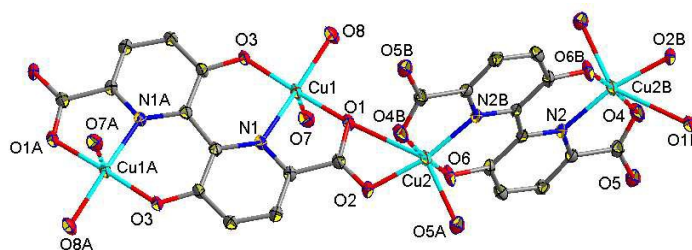
Crystal structure of 2.

The asymmetric unit consists of two crystallographically unique Cu(II) ions, two halves of hbpc⁴⁻ ligands, two coordinated water molecules. The Cu1 and Cu2 ions lie at general positions while the two halves of hbpc⁴⁻ lie about other independent inversion centers. The coordinated water molecules also occupy general positions. As shown in Figure 1a, the coordination geometry of Cu1 ion can be described as distorted square-pyramidal geometry, being bonded to two carboxylate oxygen atoms from one hbpc⁴⁻ ligand (Cu-O 1.865(2) and 1.941(2) Å, respectively), one nitrogen atom of hbpc⁴⁻ ligand (Cu-N 1.985(3) Å) and two aqua ligand (Cu-O 1.973(2) and 2.273(3) Å) (Table S1, in the Supporting Information). Cu2 ion adopts six-coordinated octahedral geometry. The equatorial is composed of two chelating carboxylate oxygen atoms, one

monodentate carboxylate oxygen atom, and monodentate nitrogen atom of two hbpdc⁴⁺ ligands. The apical positions are occupied by monodentate carboxylate oxygen atoms of hbpdc⁴⁺ ligand. The O-Cu-O and O-Cu-N angles in the equatorial plane and O-Cu-O angle along the apical direction are in the range of 85.62(10)-173.41(11)° (Table S1, in the Supporting Information), indicating the octahedron is much distorted.

In the crystal structure, one hbpdc⁴⁺ ligand in bis-(tridentate) chelating mode connects Cu1 and Cu1A, giving a dinuclear copper building block [Cu₂N₂O₂(CO₂R)₂] with short separations of Cu1...Cu1 (6.212 Å). While the other hbpdc⁴⁺ ligand also in bis-(tridentate) chelating mode links Cu2 and Cu2A, leading to the other dinuclear copper building block [Cu₂N₂O₂(CO₂R)₂] with separations of Cu2...Cu2 (6.238 Å). The former hbpdc⁴⁺ ligands in bidentate (*k*^l-*k*^l)-(*k*^l-*k*^l)-μ₂ bridging mode (Scheme 1b) connect the two adjacent but different dinuclear copper building blocks, resulting into one dimensional chains along the *a* axis with a Cu1...Cu2 distance of 4.698 Å, as depicted in Figure 1b. Additionally, it is noted that the latter hbpdc⁴⁺ ligands in bidentate (*k*^l)-(*k*^l)-μ₂ bridging mode (Scheme 1c) link the two adjacent [Cu₂N₂O₂(CO₂R)₂] building block, resulting into one dimensional chains along the *b* axis with a Cu2...Cu2 distance of 5.128 Å, as depicted in Figure 1c. The two kinds of chains are not parallel but form angles about 80° with each other. Therefore, the resulting two-dimensional sheet in the *ab* plane is formed by two kinds of chains sharing the Cu2 ions, as shown in Figure 1d.

In addition, through other hydrogen-bonding interactions originating from the coordinated water hydrogen atom and the carboxyl oxygen atom between the adjacent sheets (O...O, 2.689(3) Å, 162.1°; 2.731(3) Å, 165.9°; 2.855(3) Å, 169.3°; 2.861(3) Å, 172.0°, respectively), the 2D sheet is further linked into a 3D supramolecular network, as shown in Figure 1e. Detail of hydrogen bond interactions are brought together within Table S2 (see Supporting Information).



(a)

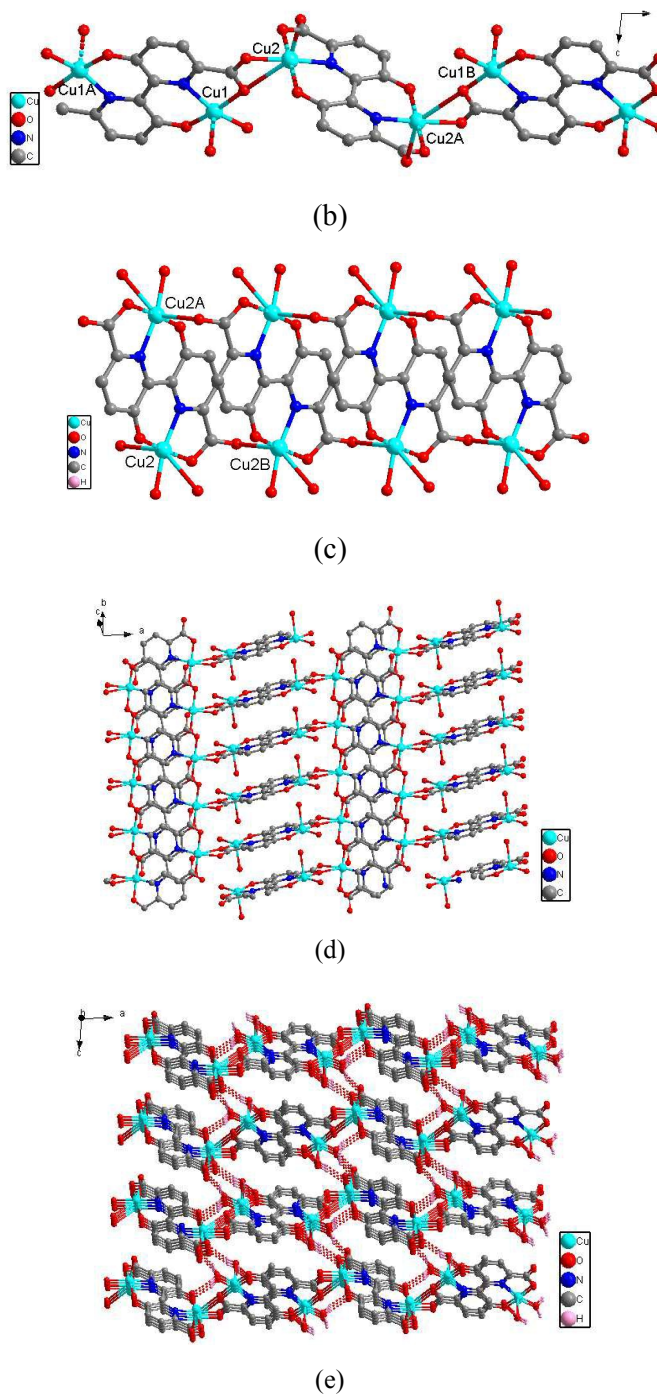
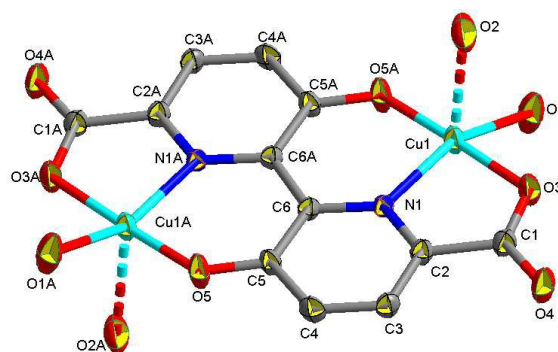


Figure 1. (a) The coordination environment of Cu(II) center in **2** with the ellipsoids drawn at the 50% probability level. The hydrogen atoms omitted for clarity (the axial long Cu-O bonds are shown as broken lines). Symmetry operators: (A) $-x+1, -y, -z+1$; (B) $-x+2, -y+1, -z+1$. (b) and (c) View of 1-D chain in **2** (the axial long Cu-O bonds are shown as broken lines). (d) View of 2-D sheet in the *ab* plane. (e) View of the 3-D supramolecular network. The extensive hydrogen bonds are colored red.

Crystal Structure of 3.

X-ray single crystal analysis of **3** indicates a discrete centrosymmetric dinuclear complex, as shown in Figure 2a. The asymmetric unit consists of one crystallographically unique Cu(II) ion, half hbpdc⁴⁺ ligand, and two coordinated water molecules. Cu(II) ion adopts five-coordinated square-pyramidal geometry, formed by one nitrogen donor and two carboxylate oxygen atoms from one hbptc⁴⁺ ligand, and two aqua ligands. The Cu–N and Cu–O bond distances lie in the range of 1.980 Å and 1.861(3)–2.291(3) Å (Table S1, in the Supporting Information), being comparable to those found for similar complexes in the literature.²⁵ For each hbpdc⁴⁺ ligand, two carboxylate groups take the same chelating coordination mode to join two Cu(II) ions (see Scheme 1d). As a result, each hbpdc⁴⁺ ligand links two Cu(II) ions to form a dinuclear unit. Within this unit, the neighboring Cu1A···Cu1B separations are 3.854 Å.

In the crystal structure of **3**, the dinuclear units are connected to each other through the formation of hydrogen bonds between the adjacent coordinated water molecules, resulting in 1D chain along the *c* axis. The adjacent chains are further connected each other through the formation of hydrogen bonds between water molecules and carboxylate oxygen atoms, resulting in a 3D supramolecular network, as shown in Figure 2b. Detail of hydrogen bond interactions are brought together within Table S2 (see Supporting Information).



(a)

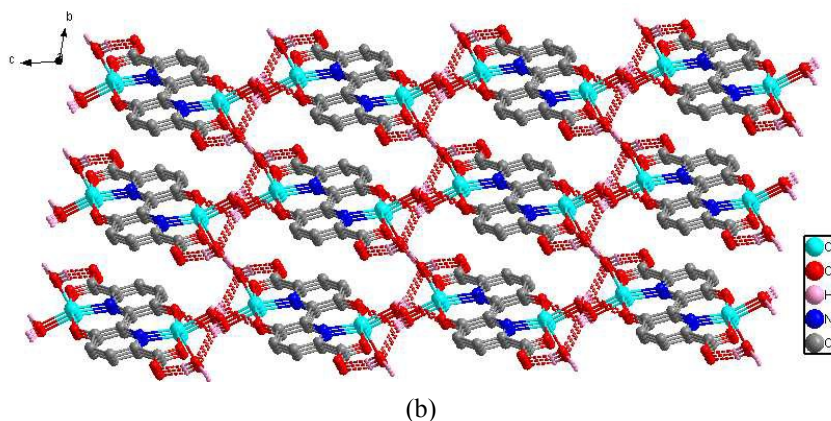


Figure 2. (a) The coordination environment of Cu(II) center in **3** with the ellipsoids drawn at the 50% probability level. The hydrogen atoms omitted for clarity (the axial long Cu-O bonds are shown as broken lines). Symmetry operators: (A) $-x, -y+1, -z+2$. (b) View of 3-D supramolecular network. The extensive hydrogen bonds are colored red.

Crystal Structure of 4.

In contrast to the above coordination polymers **1** and **2**, complex **4** is a discrete double-stranded dimer, which crystallizes in the monoclinic space group $P2_1$, and each asymmetric unit consists of two Cu(II) ions, two mhbptc^{2-} , and nine lattice water molecules. As depicted in Figure 3a, the structure of **4** is built up of dinuclear units, in which the two copper ions have the same coordination modes with $\text{Cu}\cdots\text{Cu} = 4.500(1) \text{ \AA}$. Each Cu(II) ion shows five-coordinated square-pyramidal geometry, formed by two nitrogen donor, two carboxylate oxygen atoms from two mhbptc^{2-} ligands and one pyridine nitrogen atom, in which the Cu-O bond distances range from 2.033(3) to 2.150(3) \AA , and Cu-N bond distances lie in the normal ranges of 2.196(3)–2.212(3) \AA (Table S1, in the Supporting Information). The two mhbptc^{2-} adopt bis(didentate) chelating fashions (Scheme 1e) to link two copper ions with the twist angles between two 2,2'-bipyridyl rings are 63.6(3) and 67.0(2) $^\circ$, respectively, which is significantly larger than those found in the complexes **1–3**.

Considering that there are nine lattice water molecules within the structure, the packing of complex **4** in the crystal lattice is worth mentioning. In the crystal structure of **4**, the crystalline water molecules and carboxylate oxygen atoms are the main part of hydrogen bonded motifs. The lattice water molecules contribute to bridge the adjacent double-stranded dimers to a 3D network

with hydrogen bonds, as shown in Figure 3b. The water molecules are in the interlayer space and link to each other by hydrogen bonds to form $(\text{H}_2\text{O})_{14}$ clusters. Figure 3c shows the five molecules (O4, O5, O7, O8 and O9) and their symmetric equivalents that form a ten-membered ring, which is further hydrogen bonded to a water tetramer (O2, O3, O1, O6), giving a $(\text{H}_2\text{O})_{14}$ clusters, non-bonded $\text{O}\cdots\text{O}$ distance of 2.901 Å. Similar to that observed in the reported complexes,²⁶ both water–MOF and water–water interactions can be important for the stability of the overall 3D structure of **4**. Detail of hydrogen bond interactions are brought together within Table S2 (see Supporting Information).

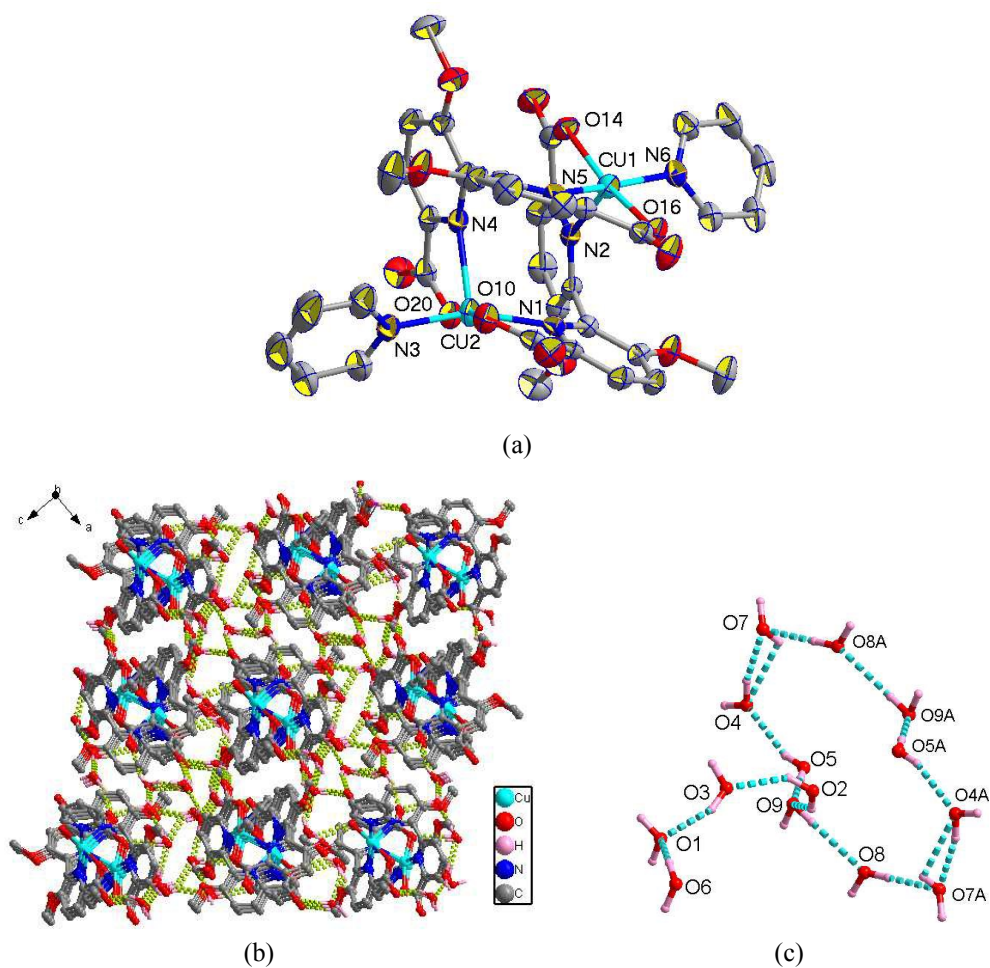


Figure 3. (a) Coordination environment of the Cu ion in **4** with the ellipsoids drawn at the 50% probability level. The hydrogen atoms and lattice water omitted for clarity. (b) View of the 3-D supramolecular network. The extensive hydrogen bonds are indicated as dotted lines. (c) View of $(\text{H}_2\text{O})_{14}$ cluster in **4** (Hydrogen bonds are indicated as dotted lines).

Crystal structure of 5.

By reducing the ligand-to-metal ratio from 1:2 to 1:1, the reaction of copper ions with mbpdcH₂ produced a mononuclear complex **5**. It is held together through the formation of hydrogen bonds among mononuclear (rather than dinuclear) copper-bpdcH₂ units. The asymmetric unit consists of one crystallographically unique Cu(II) centers, one hbpdcH₂²⁻ ion, and two coordinated water molecules, as depicted in Figure 4a. In **5**, the Cu(II) ion is also five-coordinate. Every Cu(II) ion binds simultaneously to one carboxylate oxygen, one hydroxyl oxygen and one pyridyl nitrogen from one hbpdcH₂²⁻ ion, and two aqua ligands.

In the crystal structure of **5**, the hbpdcH₂²⁻ ion adopts a tridentate chelating fashion (Scheme 1f) to bind a Cu(II) ion through adjacent one carboxylate O6, one hydroxyl O1 and one pyridine N2. The second carboxylic acid and hydroxyl functions remain uncoordinated and are unprotonated, thus neutralizing the overall positive charge of the Cu(II) ions. In the packing motif, each mononuclear is assembled via hydrogen bonding between carboxylic hydrogen and carboxylic oxygen together with the coordinated water molecules stabilizing the mononuclears which completely results to the overall 3D supramolecular structure of **5**, as shown in Figure 4b. Detail of hydrogen bond interactions are brought together within Table S2 (see Supporting Information).

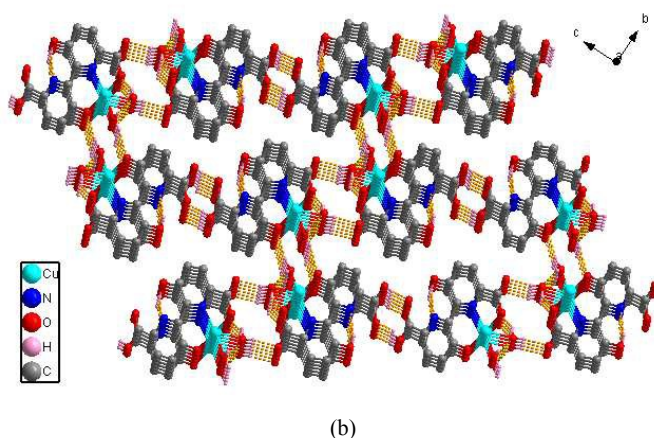
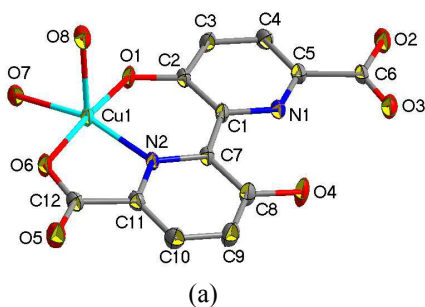


Figure 4. (a) The coordination environment of Cu(II) center in **5** with the ellipsoids drawn at the 50% probability level. The hydrogen atoms omitted for clarity. (b) View of 3D supramolecular network. The extensive hydrogen bonds are colored yellow.

Thermal Stability and Powder X-Ray Diffraction.

The pure phases of complexes **1**, **2**, **4** and **5** were confirmed by PXRD measurements, and the results are shown in Figure S1. Meanwhile, each PXRD pattern of the as-synthesized sample is consistent with the simulated one. This result shows the phase purity of the bulk samples.

The thermal stabilities of **2**, **4** and **5** were examined by thermogravimetric analysis (TGA), and the results are shown in Figure S2.

Complexes **2** and **5** undergo weight losses of 8.79% and 9.76%, respectively, which can be assigned to the losses of coordinated water molecules (calcd 8.27% for **2** and 9.63% for **5**), and the frameworks of **2** and **5** remain stable up to approximately 402 °C.

The TGA curve of **4** exhibits an initial weight loss from room temperature to 105 °C, with the observed weight loss of 15.7% corresponding to the release of lattice–water molecules (calcd 15.4%). After that an additional weight loss of 9.2% up to 293 °C may be attributed to the gradual release of coordinated pyridine molecules.

Catalytic Activity.

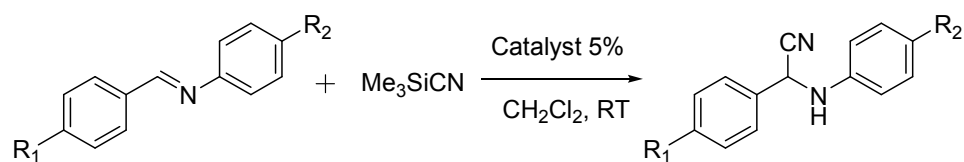
Earlier work revealed that some Cu-containing polymeric compounds were found to be good heterogeneous catalysts that offer the practical advantages of simplifying the separation and isolation of products, and of the potential for catalyst recycling.²⁷ These results have prompted us to design new Cu-containing polymeric compounds as a potential heterogeneous catalyst. The crystal structure analysis reveals there are two structural novelties in Cu-MOFs **1** and **2**. For example, both networks contain coordinatively unsaturated metal centers. In addition, the other unique feature is the observation that Cu(II) ions are coordinated by a large number of labile water molecules. These structural features encouraged us to explore possible organic transformations. As is well known, the Strecker reaction is one of the preeminent multicomponent reactions useful for the synthesis of α -amino acids via the intermediacy of α -amino nitriles.²⁸ Therefore, we examined their performance as heterogeneous catalysts for the Strecker reaction of imines under mild conditions.

To evaluate the catalytic activity of complexes **1** and **2**, these complexes were activated at 120 °C for 8 h under vacuum, to remove coordinated H₂O molecules before the reaction. Next, we used the trimethylsilyl cyanide addition to N-benzylidenebenzenamine as a test reaction (Table 2, entry 1) and afforded the corresponding α -amino nitrile as the principal product. In a typical reaction, 24 mg (0.005 mmol) sample of **1** was used for the conversion of 0.1 mmol imine in dry CH₂Cl₂ at room temperature. An excess of 50% trimethylsilyl cyanide was employed with respect to the amount of imine. Reaction conversion was monitored by checking TLC from the reaction mixture at regular time intervals. After the required reaction time, the resulting solution was filtered to remove the catalyst. The resulting solvents were evaporated in vacuum, and aqueous NaHCO₃ solution (1%, 5 mL) was added into it. The organic components were extracted into ethyl acetate, which was then dried over anhydrous Na₂SO₄. Evaporation of the solvent gave the crude product. The isolated yield was obtained by flash column chromatography on silica gel with petrol ether/ethyl acetate = 12/1 as the eluent. The product was identified by ¹H NMR analysis. Under these conditions, a smooth reaction resulted that produced the corresponding α -amino nitrile in 95% yield. The same reaction conditions were used for testing the catalytic activity of complex **2**. The results are collected in Table 2.

As can be seen from Table 3, both **1** and **2** could promote the cyanosilylation reaction between trimethylsilyl cyanide with N-benzylidenebenzenamine (entry 1), and substituted imine (entries 2–10). In the absence of networks **1** and **2**, the reaction did not proceed at all, thereby supporting the possible Lewis acidic catalyzed activity of the networks. Likewise, when the catalyst was filtered off, the reaction was no longer promoted. Further, a control experiment of using Cu(Ac)₂ as the catalyst did not result in any product formation. These control experiments strongly suggest that the soluble and catalytically active species are not leached out from both networks. Thus, the reaction was promoted by heterogeneous catalysis of complexes **1** and **2**.

Notably, the heterogeneous catalysts can be conveniently recovered from the reaction mixture by simple filtration and used several times (tested four consecutive times; entry 1, Table 2) without much loss in the catalytic efficiency (4% drop in isolated yield in the fourth run). Moreover, the recovered MOFs remained stable with complete retention of reactivity, which is further confirmed by PXRD analysis. As shown in Figure S3 and S4, the recovered material shows no change in the structure of the catalyst.

Table 2. Strecker reaction of trimethylsilyl cyanide with various imines



Entry	Imine	Yield (%) ^a	
		1	2
1		95, 93 ^b , 91 ^c	93, 91 ^b , 89 ^c
2		95	93
3		93	91
4		92	91
5		94	92
6		93	90
7		92	90
8		92	91
9		94	92
10		94	93

^a Yield based on column chromatography. ^{b,c} Isolated yield after third and fourth run, respectively.

Magnetic Properties.

The magnetic susceptibility of powdered sample of complexes **1**, **2** and **4** was measured from

2 to 300 K under a constant magnetic field of 0.1 T.

The polymer **1** displays a strong antiferromagnetic interaction. The detail discussion are reported in our previous paper.^{14d}

The magnetic susceptibilities of **2** were measured in the 2-300 K temperature range, and shown as $\chi_M T$ and χ_M versus T plots in Figure 5. The experimental $\chi_M T$ value of **2** at room temperature is $0.76 \text{ cm}^3 \text{ K mol}^{-1}$, which is close to that expected for two uncoupled Cu(II) ions ($0.75 \text{ cm}^3 \text{ K mol}^{-1}$, $S = 1/2$). The temperature dependence of the reciprocal susceptibilities ($1/\chi_M$) of **2** obey the Curie-Weiss law above 30 K with $\theta = -24.57 \text{ K}$, $C = 0.89 \text{ cm}^3 \cdot \text{K/mol}$. As temperature lowered to 2 K, the $\chi_M T$ values decrease first slowly and then rapidly. The behavior suggests that antiferromagnetic interactions are operative in **2**.

According to the structure of **2**, it could be presumed that the main magnetic interactions between the metal centers might happen between two carboxylate bridged Cu(II) ions (namely between Cu1 and Cu2), whereas the superexchange interactions between Cu(II) ions (Cu2 and Cu2) through the hbptc⁴⁻ ligands bridges can be ignored because of the long length of the hbpd⁴⁻ ligands. Therefore, the analysis of the susceptibility curves was performed using the Bleaney–Bowers formula²⁹ with the exchange Hamiltonian ($H = -JS_1S_2$, $S_1 = S_2 = 1/2$)

$$\chi_M = (2N\beta^2 g^2 / kT)[3 + \exp(-J/kT)]^{-1} (1 - \rho) + (N\beta^2 g^2 / 2kT)\rho + N_\alpha$$

Least-squares fitting of the experimental data led to $J = -13.46 \text{ cm}^{-1}$, $g = 2.04$, $\rho = 0.020$, and $R = 2.2 \times 10^{-3}$ with R defined as $\Sigma(\mu_{\text{obsd}} - \mu_{\text{calcd}})^2 / \Sigma(\mu_{\text{obsd}})^2$, where ρ is the percentage of the paramagnetic impurities, N_α the temperature-independent paramagnetism ($120 \times 10^{-6} \text{ cm}^3 \text{ mol}^{-1}$), and N, β and k have their usual meanings. The curve calculated with these parameters gave a reasonable fit to the experimental data as shown by the solid line in Figure 5.

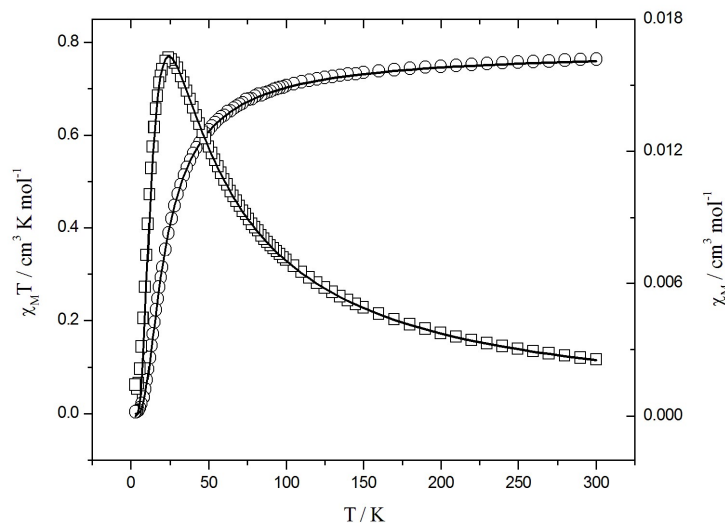


Figure 5. Temperature dependence of $\chi_M T$ and χ_M for **2**. Open points are the experimental data, and the solid line represents the best fit obtained from the Hamiltonian given in the text.

The magnetic properties of complex **4** under the form of $\chi_M T$ and χ_M versus T plots are shown in Figure 6. The experimental $\chi_M T$ value of **4** at room temperature is $0.77 \text{ cm}^3 \text{ K mol}^{-1}$, which is close to that expected for two uncoupled Cu(II) ions ($0.75 \text{ cm}^3 \text{ K mol}^{-1}$). Upon cooling, the $\chi_M T$ values remain almost constant up to 100 K, and then decreases at lower temperatures, thus complex **4** displays an overall weak antiferromagnetic coupling. The crystal structure of **4** is made up from double-stranded dimer and thus the magnetic susceptibility data can be analyzed by means of the Bleaney-Bowers equation for a copper(II) dimer.²⁹ The spin Hamiltonian defined as $H = -J(S_1 S_2)$.

$$\chi_M = (Ng^2\beta^2/3KT)[6/(3 + \exp(-J/kT))]$$

The best least-squares fit parameters are $g = 2.050(2)$, $J = -0.457(1) \text{ cm}^{-1}$, and $R = 7.285 \times 10^{-4}$. The small J value indicates a weakly antiferromagnetic interaction between the dimer.

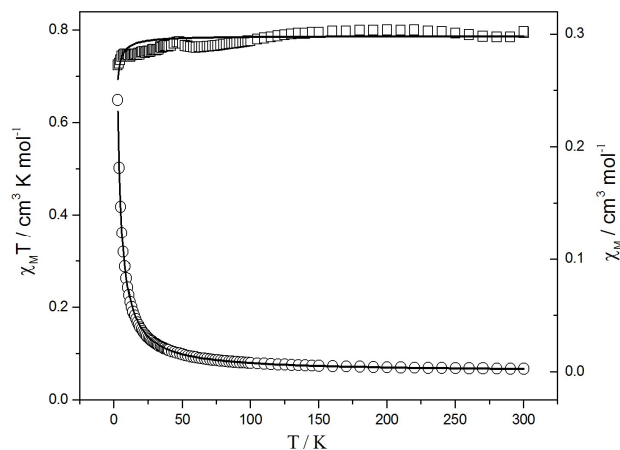


Figure 6. Temperature dependence of $\chi_M T$ and χ_M for **4**. Open points are the experimental data, and the solid line represents the best fit obtained from the Hamiltonian given in the text.

Conclusions.

In conclusion, we have carried out in situ generation of other functionality with a rigid mbptcH₂ under hydrothermal conditions to assemble five multi-functional copper(II) complexes. By fine tuning reactant ratio and reaction temperature, 3D, 2D, and 0D complexes can be acquired. Such slight modifications in the reaction conditions affect strongly the composition and structure of the obtained complexes.

The complex **1** exhibits very strong antiferromagnetic interactions, while complexes **2** and **4** display weak antiferromagnetic interactions. In **2**, the relative configuration of the hbpdCH₄ ligand with respect to the magnetic orbitals offers a poor overlap between them, while in complex **4** it is due to the lack of magnetic exchange pathway, which can clearly seen from the structural plot.

The catalytic results reveal that complexes **1** and **2**, featuring a Lewis acid-type catalytic sites, and can function as heterogeneous, very efficient and reusable catalysts for the Strecker reaction of imine.

ACKNOWLEDGMENTS

We gratefully acknowledges the financial support from the Natural Science Foundation of

China (Grant No. 21372112 and 21272109) and technology innovation team support programs of Henan Province University (No. 2012IRTSTHN019 and 14IRTSTHN008).

Supporting Information

X-ray crystallographic data for complexes **1–5** in CIF format, PXRD patterns, TGA plots, Tables for hydrogen bonds, and NMR spectra.

REFERENCES

- [1] a) B. Chen, S. Xiang, G. Dong, *Acc. Chem. Res.* **2010**, *43*, 1115–1124; b) L. Ma, C. Abney, W. Lin, *Chem. Soc. Rev.* **2009**, *38*, 1248–1256; c) M. D. Allendorf, C. A. Bauer, R. K. Bhakta, R. J. T. Houk, *Chem. Soc. Rev.* **2009**, *38*, 1330–1352; d) O. R. Evans, W. B. Lin, *Acc. Chem. Res.* **2002**, *35*, 511–522.
- [2] a) P. Mahata, S. Natarajan, *Chem. Soc. Rev.* **2009**, *38*, 2304–2318; b) J. R. Li, R. J. Kuppler, H. C. Zhou, *Chem. Soc. Rev.* **2009**, *38*, 1477–1504; c) Y. G. Huang, F. L. Jiang, M. C. Hong, *Coord. Chem. Rev.* **2009**, *253*, 2814–2834.
- [3] a) D. Sarma, P. Mahata, S. Natarajan, P. Panissod, G. Rogez, M. Drillon, *Inorg. Chem.* **2012**, *51*, 4495–4501. (b) C. S. Liu, W. Guo, E. C. Sañudo, M. Chen, M. Hu, M. Du, S. M. Fang, *CrystEngComm* **2012**, *14*, 160–168; c) T. F. Liu, J. Lü, C. B. Tian, M. N. Cao, Z. J. Lin, R. Cao, *Inorg. Chem.* **2011**, *50*, 2264–2271.
- [4] a) Z. W. Wang, C. C. Ji, J. Li, Z. J. Guo, Y. Z. Li, H. G. Zheng, *Cryst. Growth Des.* **2009**, *9*, 475–482; b) D. A. McMorran, *Inorg. Chem.* **2008**, *47*, 592–601; c) P. Mahata, S. Natarajan, *Inorg. Chem.* **2007**, *46*, 1250–1258.
- [5] a) A. Karmakar, H. M. Titi, I. Goldberg, *Cryst. Growth Des.* **2011**, *11*, 2621–2636; b) D. Sun, H. R. Xu, C. F. Yang, Z. H. Wei, N. Zhang, R. B. Huang, L. S. Zheng, *Cryst. Growth Des.* **2010**, *10*, 4642–4649; c) P. Mahata, D. Sen, S. Natarajan, *Chem. Commun.* **2008**, 1278–1280.
- [6] a) F. Luo, Y. X. Che, J. M. Zheng, *Cryst. Growth Des.* **2009**, *9*, 1066–1071; b) D. L. Reger, R. P. Watson, M. D. Smith, *Inorg. Chem.* **2006**, *45*, 10077–10087; c) Y.

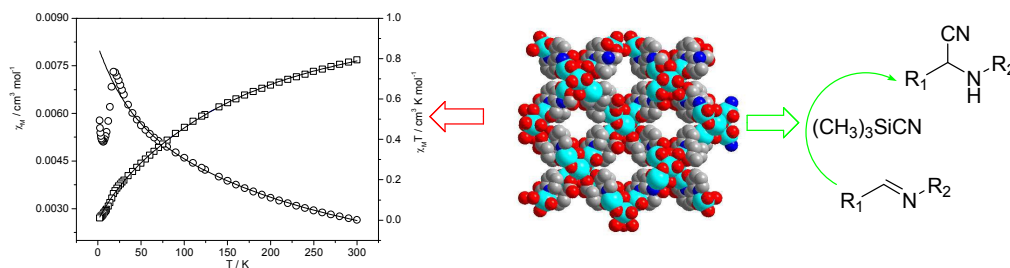
- Cui, O. R. Evans, H. L. Ngo, P. S. White, W. B. Lin, *Angew. Chem., Int. Ed.* **2002**, *41*, 1159–1162.
- [7] a) L. L. Liu, Z. G. Ren, L.W. Zhu, H. F. Wang, W. Y. Yan, J. P. Lang, *Cryst. Growth Des.* **2011**, *11*, 3479–3488; b) J. X. Chen, X. Y. Tang, Y. Chen, W. H. Zhang, L. L. Li, R. X. Yuan, Y. Zhang, J. P. Lang, *Cryst. Growth Des.* **2009**, *9*, 1461–1469; c) B. Zheng, H. Dong, J. F. Bai, Y. Li, S. Li, M. Scheer, *J. Am. Chem. Soc.* **2008**, *130*, 7778–7779.
- [8] a) Y. Liu, Y. Qi, Y. H. Su, F. H. Zhao, Y. X. Che, J. M. Zheng, *CrystEngComm* **2010**, *12*, 3283–3290; b) P. X. Yin, J. Zhang, Z. J. Li, Y. Y. Qin, Chen J. K. g, L. Zhang, Q. P. Lin, Y. G. Yao, *Cryst. Growth Des.* **2009**, *9*, 4884–4896.
- [9] a) H. X. Yang, S. Y. Gao, J. Lü, B. Xu, J. X. Lin, R. Cao, *Inorg. Chem.* **2010**, *49*, 736–744; b) L. S. Long, *CrystEngComm* **2010**, *12*, 1354–1365; c) B. X. Dong, Q. Xu, *Inorg. Chem.* **2009**, *48*, 5861–5873..
- [10] a) K. L. Zhang, C. T. Hou, J. J. Song, Y. Deng, L. Li, S. W. Ng, G. W. Diao, *CrystEngComm* **2012**, *14*, 590–600; b) F. Yu, B. Li, *CrystEngComm* **2011**, *13*, 7025–7031; c) J. Zhang, X. H. Bu, *Chem. Commun.* **2008**, 444–446; d) S. Bauer, N. Stock, *Angew. Chem., Int. Ed.* **2007**, *46*, 6857–6860.
- [11] a) G. B. Li, J. M. Liu, Y. P. Cai, C. Y. Su, *Cryst. Growth Des.* **2011**, *11*, 2763–2772; b) A. Lan, K. Li, H. Wu, D. H. Olson, T. J. Emge, W. Hong, M. Ki, J. Li, *Angew. Chem., Int. Ed.* **2009**, *121*, 2370–2374; c) S. Y. Lee, S. Park, H. J. Kim, J. H. Jung, S. S. Lee, *Inorg. Chem.* **2008**, *47*, 1913–1915.
- [12] a) W. Y. Wang, Z. L. Yang, C. J. Wang, H. J. Lu, S. Q. Zang, G. Li, *CrystEngComm.*, 2011, **13**, 4895–4902; b) F. Luo, Y. X. Che, J. M. Zheng, *Cryst. Growth Des.* **2009**, *9*, 1066–1071; c) Z. Pan, Y. Song, Y. Jiao, Z. Fang, Y. Li, H. Zheng, *Inorg. Chem.* **2008**, *47*, 5162–5168; d) K. S. Gavrilenko, O. Cador, K. Bernot, P. Rosa, R. Sessoli, S. Golhen, V. V. Pavlishchuk, L. Ouahab, *Chem. -Eur. J.* **2008**, *14*, 2034–2043.
- [13] a) S. L. Xiang, J. Huang, L. Li, J. Y. Zhang, L. Jiang, X. J. Kuang, C. Y. Su, *Inorg. Chem.* **2011**, *50*, 1743–1748; b) P. Lama, A. Aijaz, E. C. Sanudo, P. K. Bharadwaj, *Cryst. Growth Des.* **2010**, *10*, 283–290; c) X. C. Huang, W. Luo, Y. F.

- Shen, X. J. Lin, D. Li, *Chem. Commun.* **2008**, 993–995.
- [14] a) T. Zhang, C. Spitz, M. Antonietti, C. F. J. Faul, *Chem. Eur. J.* **2005**, *11*, 1001–1009; b) J. Yang, Q. Yue, G. D. Li, J. J. Cao, G. H. Li, J. S. Chen, *Inorg. Chem.* **2006**, *45*, 2857–2865; c) U. Dawid, F. P. Pruchnik, R. Starosta, *Dalton Trans.* **2009**, 3348–3353; d) B. M. Ji, D. S. Deng, H. H. Lan, C. X. Du, S. L. Pan, B. Liu, *Cryst. Growth Des.* **2010**, *10*, 2851–2853; e) B. M. Ji, D. S. Deng, X. He, B. Liu, S. B. Miao, N. Ma, W. Z. Wang, L. G. Ji, P. Liu, X. F. Li, *Inorg. Chem.* **2012**, *51*, 2170–2177.
- [15] a) Y. H. Liu, Y. L. Lu, H. C. Wu, J. C. Wang, K. L. Lu, *Inorg. Chem.* **2002**, *41*, 2592–2597; b) D. Bradshaw, J. B. Claridge, E. J. Cussen, T. J. Prior, M. J. Rosseinsky, *Acc. Chem. Res.* **2005**, *38*, 273–282; c) J. Y. Wu, T. T. Yeh, Y. S. Wen, J. Twu, K. L. Lu, *Cryst. Growth Des.* **2006**, *6*, 467–473; d) N. R. Kelly, S. Goetz, S. R. Batten, P. E. Kruger, *CrystEngComm.* **2008**, *10*, 1018–1026.
- [16] a) R. J. Kuppler, D. J. Timmons, Q. R. Fang, J. R. Li, T. A. Makal, M. D. Young, D. Q. Yuan, D. Zhao, W. J. Zhuang, H. C. Zhou, *Coord. Chem. Rev.* **2009**, *253*, 3042–3066; b) D. J. Tranchemontagne, J. L. Mendoza-Cortes, M. O’Keeffe, O. M. Yaghi, *Chem. Soc. Rev.* **2009**, *38*, 1257–1283; d) Z. Wang, G. Chen, K. L. Ding, *Chem. Rev.* **2009**, *109*, 322–359.
- [17] a) K. Ohara, M. Kawano, Y. Inokuma, M. Fujita, *J. Am. Chem. Soc.* **2010**, *132*, 30–31; b) A. Corma, H. Garcia, F. X. L. Xamena, *Chem. Rev.* **2010**, *110*, 4606–4655; c) T. Uemura, Y. Ono, Y. Hijikata, S. Kitagawa, *J. Am. Chem. Soc.* **2010**, *132*, 4917–4924; d) A. P. Singh, G. Kumar, R. Gupta, *Dalton Trans.* **2011**, *40*, 12454–12461; e) G. Kumar, R. Gupta, *Inorg. Chem.* **2012**, *51*, 5497–5499.
- [18] SHELXTL, Version 5.1; Bruker AXS: Madison, WI, 1998.
- [19] Sheldrick, G. M. *SHELXS-97 and SHELXL-97, Program for X-ray Crystal Structure Solution*, University of Göttingen, Germany, 1997.
- [20] a) H. B. Zhu, S. H. Gou, *Coord. Chem. Rev.* **2011**, *255*, 318–338; b) H. Zhao, Z. R. Qu, H. Y. Ye, R. G. Xiong, *Chem. Soc. Rev.* **2008**, *37*, 84–100; c) X. M. Chen, M. L. Tong, *Acc. Chem. Res.* **2007**, *40*, 162–170.

- [21] a) D. S. Li, P. Zhang, J. Zhao, Z. F. Fang, M. Du, K. Zou, Y. Q. Mu, *Cryst. Growth. Des.* **2012**, *12*, 1697–1702; b) Y. P. Wu, D. S. Li, F. Fu, W. W. Dong, J. Zhao, K. Zou, Y. Y. Wang, *Cryst. Growth. Des.* **2011**, *11*, 3850–3857; c) E. Nauha, A. Ojala, M. Nissinen, H. Saxell, *CrystEngComm* **2011**, *13*, 4956–4964.
- [22] a) D. S. Deng, L. L. Liu, B. M. Ji, G. J. Yin, C. X. Du, *Cryst. Growth. Des.* **2012**, *12*, 5338–5348; (b) Z. G. Li, G. H. Wang, H. Q. Jia, N. H. Hu, J. W. Xu, *CrystEngComm* **2007**, *9*, 882–887.
- [23] B. Zhao, P. Cheng, X. Y. Chen, C. Cheng, W. Shi, D. Z. Liao, S. P. Yan, Z. H. Jiang, *J. Am. Chem. Soc.* **2004**, *126*, 3012–3013.
- [24] Spek, A. L. *PLATON99, A Multipurpose Crystallographic Tool*; Utrecht University: Utrecht, The Netherlands, 1999.
- [25] a) J. Boonmak, S. Youngme, N. Chaichit, G. A. van Albada, J. Reedijk, *Cryst. Growth Des.* **2009**, *9*, 3318–3326; b) Y. Y. Karabach, A. M. Kirillov, M. Haukka, J. Sanchiz, M. N. Kopylovich, A. J. L. Pombeiro, *Cryst. Growth Des.* **2008**, *8*, 4100–4108.
- [26] a) A. H. Yang, H. Zhang, H. L. Gao, W. Q. Zhang, L. He, J. Z. Cui, *Cryst. Growth Des.* **2008**, *8*, 3354–3359; b) U. Mukhopadhyay, I. Bernal, *Cryst. Growth Des.* **2006**, *6*, 363–365.
- [27] a) H. X. Li, W. Zhao, H. Y. Li, Z. L. Xu, W. X. Wang, J. P. Lang, *Chem. Commun.* **2013**, *49*, 4259–4261; b) Z. Q. Xu, Q. Wang, H. J. Li, W. Meng, Y. Han, H. W. Hou, Y. T. Fan, *Chem. Commun.* **2012**, *48*, 5736–5738; c) I. H. Hwang, J. M. Bae, W. S. Kim, Y. D. Jo, C. Kim, Y. Kim, S. J. Kim, S. Huh, *Dalton Trans.* **2012**, *41*, 12759–12765.
- [28] a) A. M. Seayad, B. Ramalingam, K. Yoshinaga, T. Nagata, C. L. L. Chai, *Org. Lett.* **2010**, *12*, 264–267; b) M. Hatano, Y. Hattori, Y. Furuya, K. Ishihara, *Org. Lett.* **2009**, *11*, 2321–2324; c) J. Jarusiewicz, Y. Choe, K. S. Yoo, C. P. Park, K. W. Jung, *J. Org. Chem.* **2009**, *74*, 2873–2876; d) R. Reingruber, T. Baumann, S. Dahmen, S. Broese, *Adv. Synth. Catal.* **2009**, *351*, 1019–1024.
- [29] Kahn, O. *Molecular Magnetism*; VCH Publishers: New York, 1993.

In Situ Generation of Functionality in a Reactive Binicotinic-Acid-Based Ligand for the Design of Multi-Functional Copper(II) Complexes: Syntheses, Structures and Properties

Dongsheng Deng,^a Hui Guo,^a Guohui Kang,^{a,b} Lufang Ma,^a Baoming Ji^{a*}



Five copper binicotinic complexes including two coordination polymers, one dinuclear, one dimer, and one mononuclear copper(II) have been synthesized using an in situ generation functional ligands depending on the reaction conditions. Both of the two coordination polymers exhibit antiferromagnetic interactions as well as excellent catalytic activity for Strecker reaction of imines.